nature communications

Article

https://doi.org/10.1038/s41467-025-57231-9

Reversible ubiquitination conferred by domain shuffling controls paired NLR immune receptor complex homeostasis in plant immunity

Received: 1 July 2024

Accepted: 13 February 2025

Published online: 26 February 2025

Check for updates

Zhiyi Chen[1,3], Jianhua Huang[2,3], Jianyu Li[1], Frank L. H. Menke[2], Jonathan D. G. Jones[2] ✉ & Hailong Guo[1] ✉

Plant intracellular NLR immune receptors can function individually or in pairs to detect pathogen effectors and activate immune responses. NLR homeostasis has to be tightly regulated to ensure proper defense without triggering autoimmunity. However, in contrast to singleton NLRs, the mechanisms controlling the paired NLRs complex homeostasis are less understood. The paired Arabidopsis RRS1/RPS4 immune receptor complex confers disease resistance through effector recognition mediated by the integrated WRKY domain of RRS1. Here, through proximity labeling, we reveal a ubiquitination-deubiquitination cycle that controls the homeostasis of the RRS1/RPS4 complex. E3 ligase RARE directly binds and ubiquitinates RRS1's WRKY domain to promote its proteasomal degradation, thereby destabilizing RPS4 indirectly and compromising the stability and function of the RRS1/RPS4 complex. Conversely, the deubiquitinating enzymes UBP12/UBP13 deubiquitinate RRS1's WRKY domain, counteracting RARE's effects. Interestingly, the abundance of WRKY transcription factors WRKY70 and WRKY41 is also regulated by RARE and UBP12/UBP13. Phylogenetic analysis suggests this regulation likely transferred from WRKY70/WRKY41 to RRS1 upon WRKY domain integration. Our findings improve our understanding of homeostatic regulation of paired NLR complex and uncover a paradigm whereby domain integration can co-opt preexisting post-translational modification to regulate novel protein functions.

Phytopathogens secrete effector proteins into plant cells to suppress plant immunity for colonization. To circumvent pathogen invasion, plants have evolved intracellular nucleotide-binding leucine-rich repeat immune receptors (NLRs) that recognize effectors, either by directly binding effectors or by monitoring effector-mediated modification of "guardees" or "decoys" to activate effector-triggered immunity (ETI). Activation of ETI involves calcium influx, global transcriptional reprogramming and programmed cell death called hypersensitive response (HR)[1,2]. Canonical NLRs contain a C-terminal leucine-rich repeat (LRR) domain, a central nucleotide-binding (NB) domain and a variable N-terminal domain including Toll/Interleukin-1 receptor (TIR) domain, coiled-coil (CC) domain, or Resistance to

[1]State Key Laboratory of Agricultural and Forestry Biosecurity, Department of Plant Pathology, China Agricultural University, Beijing, China. [2]The Sainsbury Laboratory, University of East Anglia, Norwich Research Park, Norwich, UK. [3]These authors contributed equally: Zhiyi Chen, Jianhua Huang.
✉e-mail: jonathan.jones@tsl.ac.uk; hailongguo@cau.edu.cn

Powdery Mildew 8 (RPW8)-like CC (CC_R) domain[3]. Based on their N-termini, NLRs are classified into TNLs (TIR-NLRs), CNLs (CC-NLRs) and RNLs (CC_R-NLR). Upon effector recognition, both CNLs and TNLs oligomerize into complexes termed resistosomes that activate their calcium-permeable ion channel activity or NADase combined with ribosyl-transferase activities, respectively, with the latter producing small molecules that contribute to RNL activation[4–7].

A subclass of NLRs carries additional noncanonical domain(s) that appear to have evolved by integrating authentic effector targets into the canonical NLR structure. These NLRs with extra domains are thus commonly referred to as NLRs with integrated domains (NLR-IDs) that account for around 10-15% of the NLRome of many plant species[8,9]. Several functionally characterized NLR-IDs require another genetically linked canonical NLR to work in pairs for their function and are therefore known as NLR pairs (or sensor-executor pairs)[3,10]. Sensor and executor NLRs form pre-activation complexes in the resting state and, upon binding of effectors to the integrated domains, sensor NLRs undergo a series of intra- and intermolecular conformational rearrangements that relay effector perception to the executor NLRs for immune signaling initiation[11–13]. The Arabidopsis RRS1/RPS4 immune receptor complex, one of the best-studied paired NLRs, confers resistance to bacterial pathogens *Pseudomonas syringae* pv. *pisi*. and *Ralstonia solanacearum* by recognizing effectors AvrRps4 and PopP2, respectively[14]. RRS1 from Arabidopsis accession Col-0 (termed RRS1-S) recognizes only AvrRps4, while the RRS1 from accessions Nd-1 and Ws-2 (termed RRS1-R), with a longer C-terminal extension beyond the end of the WRKY domain compared to RRS1-S, confers responsiveness to both AvrRps4 and PopP2[15,16]. AvrRps4 and PopP2 are both detected by the C-terminal integrated WRKY domain of RRS1-R that mimics the authentic targets of effectors and derepress the complex in distinct ways[17,18]. Whether the WRKY ID possesses additional roles in controlling immune activation and regulation of RRS1/RPS4 complex remains uncharacterized.

In recent years, it became apparent that NLRs are associated with NLR-interacting proteins to achieve a balanced level of immunity[19]. Ubiquitination, a reversible and dynamic process of tagging ubiquitin to a substrate protein, plays a pivotal role in maintaining NLRs homeostasis. A few E3 ligases were found to associate with NLRs to regulate their protein degradation via 26S proteasome. For example, the F-box containing E3 ligase CPR1 was shown to target NLR proteins SNC1, RPS2 and SUMM2 for degradation[20,21]. Two functionally redundant RING-type E3 ligases, MUSE1/MUSE2, regulate the turnover of SNC1's partners, SIKIC1/2/3[22]. Interestingly, another two closely related RING-type E3 ligases, SNIPER1/SNIPER2, broadly regulate the homeostasis of diverse sensor NLRs including SNC1, SUMM2, RPP4 and RPM1[23]. However, all E3 ligases that have been identified to date are from the investigations of single NLR proteins. Furthermore, to date, no deubiquitinating enzymes have been identified that directly remove ubiquitin from NLRs and limit their 26S proteasomal degradation.

NLR-ID fusion proteins are likely formed through DNA transposition and/or ectopic recombination, the major contributors to domain shuffling[24]. Domain shuffling constantly occurred during the dynamic evolutionary history of NLRs and facilitated the diversity of NLR repertoires, allowing NLRs to cope with the rapid evolution of pathogen effectors. Fusion of effector-targeted domains into NLRs via domain shuffling creates NLR-IDs that can reveal the action of effectors[25,26]. As more paired NLR/NLR-ID complex have now been identified, how such NLR/NLR-ID complexes are regulated and how domain shuffling affects fusion proteins regulation remains unknown. In this study, using TurboID-based proximity labeling, we identified the E3 ligase RARE that associates with RRS1/RPS4 complex through directly interacts with RRS1 but not with RPS4. RARE targets RRS1 for ubiquitination through the WRKY domain and destabilizes the complex abundance in a RRS1-dependent manner, thus suppressing immune responses conditioned by RRS1/RPS4. Additionally, we found that two closely related deubiquitinating enzymes UBP12/UBP13 antagonize the action of RARE through deubiquitinating RRS1. Interestingly, RARE and UBP12/UBP13 also modulate the homeostasis of WRKY transcription factors WRKY70 and WRKY41. Phylogenetic analysis suggests that such regulation was most likely transferred from the WRKY transcription factors to RRS1 during WRKY domain integration. Thus, our findings not only uncover the reversible ubiquitination of ID in regulating the homeostasis of paired NLR/NLR-ID complex, but also reveal a paradigm whereby domain integration can transfer pre-existing post-translational regulatory mechanisms like ubiquitination to regulate novel protein functions.

Results

Identification of RARE and UBP12/UBP13 in the proxiomes of RRS1

To unravel the regulation and signaling of RRS1/RPS4 immune receptor complex, we employed proximity labeling to identify their interactors[27]. Both RRS1 and RPS4 were fused with highly active biotin ligase TurboID tagged with a FLAG epitope for proximity labeling. In biotinylation assays, RRS1-TurboID induced more pronounced biotinylation compared to RRS4-TurboID in *Nicotiana benthamiana* (*Nb*), likely due to its higher protein abundance (Supplementary Fig. 1A). Alongside cognate effectors AvrRps4 and PopP2, co-expression of RRS1 and RPS4 triggers HR in *N. tabacum*. However, the fusion of the TurboID tag impaired the HR only when fused to RPS4 but not RRS1 (Fig. 1A), suggesting that RRS1-TurboID, but not RPS4-TurboID, is fully functional. Consistently, resistance against *Pseudomonas syringae* (*Pst*) DC3000 carrying AvrRps4 was restored in Col-0 *rrs1arrs1b* mutants complemented with the RRS1-TurboID transgene driven by pAt2 promoter (Fig. 1B and C), which allows moderate constitutive expression[28,29]. We therefore utilized RRS1-R-TurboID for further proximity labeling assays since RRS1-S is likely a derived allele from RRS1-R as a result of premature stop codon[15,16].

RPS4 and PopP2 are known to interact with RRS1[14,30]. To assess the specificity of TurboID-based proximity labeling, RPS4 or PopP2 was co-expressed with TurboID-tagged RRS1-R in *Nb* leaves followed by immunoprecipitation and biotinylation detection. Clear biotinylation signals were observed for RPS4 and PopP2 in the presence of TurboID-tagged RRS1-R but not negative control mCherry (Fig. 1D and Supplementary Fig. 1B), indicating the high specificity of TurboID-based proximity labeling. Notably, consistent with our previous studies[14], RRS1-R was not co-precipitated with PopP2, likely due to their weak or transient acetyltransferase–substrate interactions (Supplementary Fig. 1B). This finding supports the notion that proximity labeling outperforms affinity precipitation in identifying interactors with weak and transient interaction.

We then employed the *pAT2-RRS1-R-TurboID-FLAG* complementation in Col-0 *rrs1arrs1b* for the proximity-labeling proteomics. Wild-type plants expressing GFP carrying a nuclear localization signal (NLS) and TurboID-FLAG tag served as a negative control, as RRS1-R localizes in the nucleus[16]. In agreement with previous reports[31], TurboID produced background labeling without the addition of exogenous biotin but the labeling yield can be further strongly increased in the presence of exogenous biotin. Biotin treatment of transgenic seedlings induced the overall biotinylation output signal (Fig. 1E). The total biotinylated proteins were enriched using streptavidin-conjugated beads (Fig. 1F) and analyzed via liquid chromatography-tandem mass spectrometry (LC-MS) analysis. Proteins showing >three-fold higher peptide spectrum count in the RRS1-R-TurboID samples versus the GFP-TurboID samples were considered as RRS1-proximal proteins, leading to 273 candidates (Supplementary Data 1). Notably, among them are RPS4, a known interactor of RRS1-R, and regulators of plant NLRs, including Topless-related (TPR) proteins,

https://doi.org/10.1038/s41467-025-57231-9

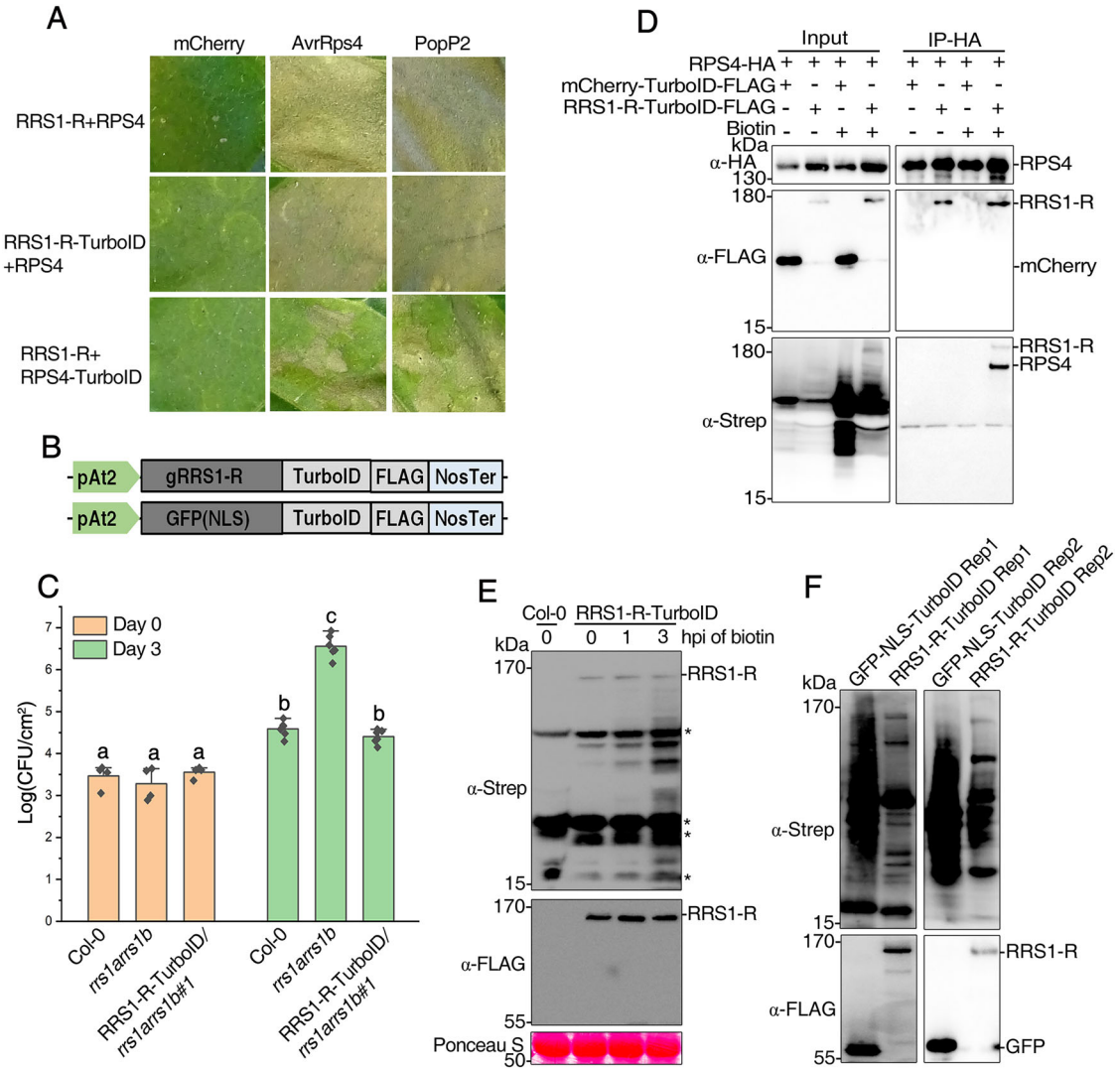

Fig. 1 | Establishment of TurboID-mediated proximity labeling in Arabidopsis for identification of proximal proteins of RRS1/RPS4 complex. A Analysis of ability of RRS1-R-TurboID or RPS4-TurboID construct to induce cell death in response to AvrRps4 or PopP2. Each tobacco leaf section was coinfiltrated to transiently express the indicated constructs together with either mCherry, AvrRps4 or PopP2. Photograph was taken at 4 days post infiltration (dpi). **B** Diagram of the expression cassettes used for the expression of TurboID. GFP containing a NLS was fused to the N-terminus while a FLAG tag was added to the C-terminus of TurboID. Expression was under the control of Arabidopsis SSR16 (Small Subunit Ribosomal Protein 1 promoter, named as pAt2 in TSL 'moderate promoter' database for moderate expression in Arabidopsis) and nopaline synthase terminator. **C** RRS1-R-TurboID fusion protein complements loss of resistance to *Pst* DC3000 (AvrRps4) observed in the *rrs1arrs1b* mutant. Bacterial growth was measured 3 days post infiltration (dpi). Data are shown as means ± SD ($n = 4$ and 6 biological replicates, respectively). The corresponding p values can be found in the Source Data. **D** TurboID-based analysis of RPS4 biotinylation by RRS1-R-TurboID in *Nb*. *Nb* leaves were agroinfiltrated with the indicated constructs and biotin was infiltrated into the previously agroinfiltrated leaves at 36 h post-agroinfiltration (hpi). mCherry-TurboID served as a negative control. IP was carried out using samples collected 3 h after biotin treatment with anti-HA beads. The FLAG-tagged proteins were detected using anti-FLAG antibody and biotinylated proteins were detected using Streptavidin-HRP antibody, respectively. **E** Biotinylation of RRS1-R and its vicinal proteins in RRS1-R-TurboID transgenic plants. Total protein extracts from seedlings with or without biotin treatment were immunoblotted with Streptavidin-HRP and anti-FLAG antibody for detection of biotinylated proteins (top panel) and expression of TurboID (lower panel), respectively. Non-treated seedlings were used as controls to visualize the background activity of TurboID with endogenous biotin. Col-0 seedlings served as a control. The asterisks indicate the positions of naturally biotinylated proteins. **F** Streptavidin pull-down analysis of biotinylated proteins by TurboID-tagged RRS1-R. GFP-fused TurboID served as a control. Immunoblotting analysis of the Streptavidin pull-down products were probed with Streptavidin-HRP (top panel) and anti-FLAG antibody (lower panel).

MAC1 and MAC5A, suggesting the reliability of our data[32,33]. The balanced action of E3 ubiquitin ligases and deubiquitinases determines protein levels and activity[34]. A previously reported, but functionally uncharacterized E3 ubiquitin ligase (AT1G18660, hereafter referred as RARE, RRS1-associated RING-type E3 ligase) and two redundant deubiquitinating enzymes (DUBs), ubiquitin-specific protease 12 (UBP12) and UBP13 are also among the candidates. Given the preliminary evidence for their involvement in plant immunity and their elusive nature on homeostasis regulation[35,36], we focused on further investigations of RARE and UBP12/UBP13.

RARE is an E3 ubiquitin ligase that interacts directly with RRS1 and indirectly with RPS4 via RRS1

RARE contains a C3HC4-type RING domain with eight metal-binding residues (7 Cys and 1 His) coordinating two zinc ions in a cross-brace arrangement (Supplementary Fig. 2), indicative of a potential E3 ubiquitin ligase[37]. A common feature of most E3 ligases is their ability to autoubiquitinate. In vitro ubiquitination assays revealed that RARE underwent autoubiquitination and also generated unanchored poly-Ub, while the RARE^{H213Y} variant (Fig. 2A), harboring a tyrosine substitution of the zinc-binding histidine 213 (H213Y), did not (Figs. 2A,

https://doi.org/10.1038/s41467-025-57231-9

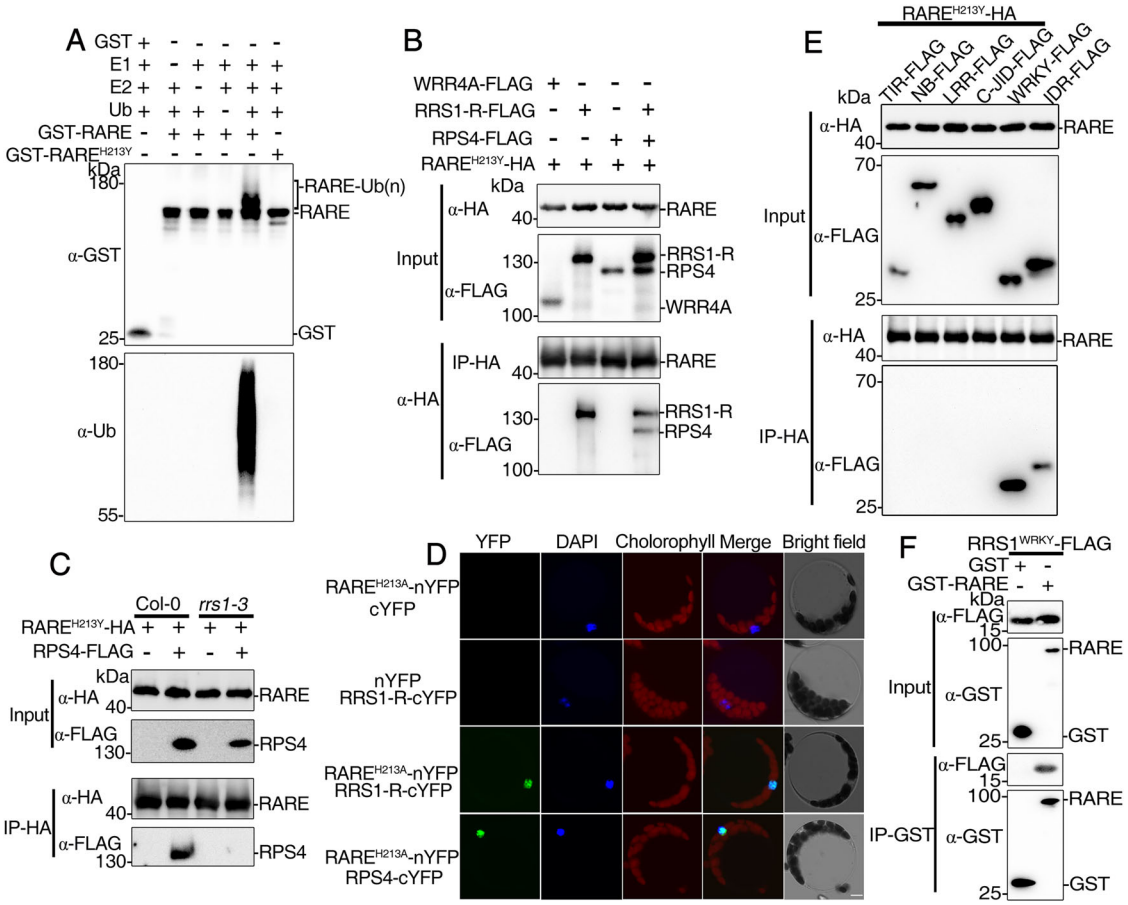

Fig. 2 | RARE is an E3 ubiquitin ligase that interacts directly with RRS1 and indirectly with RPS4 via RRS1. A Assays of in vitro self-ubiquitination of RARE. GST-RARE and GST-RARE^{H213Y} were assayed for E3 activity in the presence of E1 (UBA2), E2 (UBC10), ubiquitin (Ub) and ATP. "+" and "-" denote the presence or absence of the components of each reaction mixture. GST served as a negative control. The presence of RARE or RARE^{H213Y} was detected using anti-GST antibody (upper panel). Protein ubiquitination bands generated by GST-RARE are indicated on the right. Ubiquitination results in a heterogeneous collection of higher molecular mass proteins that are detected with anti-ubiquitin antibody (lower panel). **B** Co-IP assays reveal that the interaction of RARE with RRS1/RPS4 complex is dependent on RRS1. Samples were harvested from *Nb* transiently coexpressing FLAG-tagged RRS1/RPS4 and HA-tagged RARE. Total extracts were immunoprecipitated with anti-HA antibody-coupled beads followed by immunoblotting with the indicated antibody. WRR4A served as a control. **C** Co-IP assays for the interaction of RARE with RPS4 in protoplasts from Col-0 and *rrs1-3* plants. Protoplasts from Col-0 and *rrs1*-3 co-transfected with the RARE-HA and RPS4-FLAG constructs were incubated overnight, and total protein extracts were subjected to immunoprecipitation with anti-HA antibody-coupled beads followed by immunoblotting using either anti-HA or anti-FLAG antibody. **D** BiFC analyses for the interaction of RARE with RRS1/RPS4 complex in Col-0 protoplasts. Protoplasts were transformed with the indicated BiFC constructs and YFP fluorescence was visualized by confocal microscopy 16-20 h after transient expression. The positions of nuclei were shown by 4, 6-diamidino-2-phenylindole (DAPI) staining. Scale bar, 5 μm. **E** Co-IP assays to evaluate the association of RARE with individual domain of RRS1-R after transient co-expression in *Nb*. Total protein extracts were subjected to immunoprecipitation with agarose-conjugated anti-HA antibody followed by immunoblot analysis using either anti-HA or anti-FLAG antibody. **F** Pull-down assay for the interaction of RARE with WRKY domain of RRS1. FLAG-tagged WRKY was incubated with immobilized GST or GST-tagged RARE. After washing, bound proteins were eluted and subjected to immunoblot analysis using anti-FLAG antibody.

Supplementary Fig. 2). These results indicate that RARE is an active E3 ligase.

The identification of RARE from proximity labeling proteomics prompted us to test its interaction with RRS1-R and RPS4. We performed co-immunoprecipitation (Co-IP) assays after transient coexpression of E3 ligase activity-deficient RARE^{H213Y} with RRS1-R or RPS4 in *Nb* since a functional E3 ligase might destabilize its substrate and reduce protein-protein interactions strength[38]. RARE^{H213Y} interacted with RRS1-R but not with RPS4 and the negative control TNL protein WRR4A (White Rust Resistance 4 A)[39] (Fig. 2B). RRS1 was not co-immunoprecipitated with the GFP negative control, excluding the possibility that RRS1 is a sticky protein associating non-specifically with RARE (Supplementary Fig. 3A). However, the interaction between RARE^{H213Y} and RPS4 could only be observed in the presence of RRS1-R (Fig. 2B), suggesting that RARE interacts with RPS4 via RRS1-R. The RRS1-dependent RARE-RPS4 interaction was further supported by finding that RPS4 associated with RARE^{H213Y} in Co-IPs conducted in Arabidopsis protoplast derived from wild-type plants but not from the *rrs1–3* mutants that lack the endogenous RRS1 proteins[29](Fig. 2C). Consistently, the bimolecular fluorescence complementation (BiFC) assays showed that RARE^{H213Y} interacts with RPS4 in protoplasts derived from wild-type plants but not from the *rrs1–3* mutants, while its association with RRS1-R was observed in nucleus (Figs. 2D and Supplementary Fig. 3B). This agrees with the nuclear localization of RRS1-R and the nucleocytoplasmic localization of RARE (Supplementary Figs. 4A, B).

To identify the domain of RRS1-R responsible for RARE interaction, we performed Co-IPs in *Nb* by co-expressing RARE^{H213Y} with individual domains of RRS1-R. In the Co-IP assays, HA-tagged RARE^{H213Y}, but not the GFP negative control, interacts strongly with the WRKY domain and weakly with intrinsically disordered region (IDR) but not with other domains of RRS1-R (Figs. 2E, Supplementary Fig. 5). As IDRs

are prone to forming weak promiscuous interactions due to their high flexibility[40], we conclude that RARE interacts with RRS1-R primarily through the WRKY domain. In vitro pull-down assays showed that the WRKY of RRS1-R directly binds to RARE^{H213Y} (Fig. 2F), indicative of a direct interaction between RARE and RRS1-R. Collectively, these data suggest that RARE interacts directly with RRS1-R primarily through its RRS1-R^{WRKY}, and indirectly with RPS4 via RRS1.

RARE ubiquitinates RRS1 through its integrated WRKY domain

The direct interaction between RARE and RRS1 led us to examine whether RARE ubiquitinates RRS1. When co-expressed in *Nb*, RRS1-R was ubiquitinated by RARE but not the E3 ligase-dead RARE^{H213Y} variant (Fig. 3A), suggesting that RRS1-R is ubiquitinated by RARE. To confirm this in Arabidopsis, we obtained the *rare* mutant (a T-DNA null mutant of *RARE*, Supplementary Figs. 6A, B), and crossed it into wild-type plants expressing *pAT2::RRS1-R-FLAG* generated by our previous study[18]. Ubiquitinated RRS1-R was detected in the *pAT2::RRS1-R-FLAG* transgenic lines, while the introduction of *RARE* knockout almost abolished RRS1-R ubiquitination (Fig. 3B). Furthermore, following immunoprecipitation using agarose beads conjugated with ubiquitin antibody, the detected ubiquitination of RRS1 was weaker in *rare* than in Col-0 plants (Supplementary Fig. 6C).Collectively, these results indicate that RARE ubiquitinates RRS1-R.

Since the interaction with RARE is primarily mediated by the integrated WRKY domain of RRS1-R, we next tested whether RARE could directly ubiquitinate RRS1-R^{WRKY}. In vitro ubiquitination assays showed that RRS1-R^{WRKY} was ubiquitinated by RARE but not by RARE^{H213Y} (Fig. 3C). Additionally, RARE ubiquitinated RRS1-R but not the RRS1-R$^{\Delta WRKY}$ variant lacking the WRKY ID when co-expressed in *Nb* (Fig. 3D). These data suggest that RARE ubiquitinates RRS1-R through its WRKY domain.

Many Arabidopsis accessions carry RRS1B/RPS4B, an RRS1/RPS4 paralogous pair with similar domain architecture. The WRKY domains of RRS1B and RRS1 share ~60% amino acid sequence identity[29]. Like RRS1-R, we found that both RRS1B and RRS1B^{WRKY} can be ubiquitinated by RARE (Supplementary Figs. 7A, B). These data suggest that RARE ubiquitinates RRS1 and its paralogue RRS1B through their integrated WRKY domains.

RARE destabilizes RRS1/RPS4 complex in a RRS1-dependent manner and negatively regulates RRS1/RPS4–mediated defense responses

E3 ligase-catalyzed ubiquitination often targets substrates for proteasomal degradation[41]. As RARE ubiquitinates RRS1-R, we tested its effect on RRS1/RPS4 complex abundance. When co-expressed in *Nb*, accumulation of RRS1-R was impaired by RARE. Intriguingly, RARE destabilized RPS4 only when co-expressed with RRS1-R, but not RPS4 alone (Fig. 4A). This destabilization requires RARE's ubiquitin ligase activity, as RARE^{H213Y} failed to reduce the complex levels (Supplementary Fig. 8). Consistent with our previous studies[42,43], we found that RRS1 stabilized RPS4 (Fig. 4A). RARE likely destabilizes RPS4 by promoting RRS1-R degradation, thereby disrupting RRS1-R-mediated stabilization of RPS4. Supporting this, transiently expressing RARE reduced the protein abundance of RPS4 in wild-type but not *rrs1–3* Arabidopsis protoplasts (Fig. 4B). Collectively, these results demonstrate that RARE negatively regulates RRS1/RPS4 complex abundance in an RRS1-dependent manner.

To verify RARE's homeostatic control of the RRS1/RPS4 complex in Arabidopsis, we generated *RARE*-overexpressing transgenic lines driven by the constitutive 35S promoter (*RAREOE*, Supplementary Figs. 9A, B) and crossed the *RAREOE* transgene and the *rare* null allele into the epitope-tagged RRS1-R/RPS4 transgenic lines (*pAT2::RRS1-R-FLAG/pAT3::RPS4-HA*) generated by a previous study[18]. RRS1 and RPS4 abundance considerably increased in *rare* but decreased in *RAREOE* background (Fig. 4C), while *RRS1-R* transcripts remained similar (Supplementary Fig. 10A), suggesting that RARE post-translationally modulates RRS1/RPS4 complex levels. Cycloheximide (CHX) chase assays revealed slower degradation of RRS1-R/RPS4 complex in *rare* than in wild-type background and the degradation was inhibited by the 26S proteasome inhibitor MG132 (Supplementary Figs. 10B, C). Taken together, these results demonstrate that RARE regulates RRS1/RPS4 abundance by mediating RRS1 degradation via the 26S proteasome machinery.

RARE's homeostatic control of the RRS1/RPS4 complex prompted us to test its role in regulating RRS1/RPS4–mediated defense responses. Tobacco transient expression showed that RARE abolished HR triggered by RRS1/RPS4 in recognition of AvrRps4 (Fig. 4 D). RRS1-R^{slh1} and RRS1-R^{T1214A} are two auto-active alleles of RRS1-R that carry mutations in the WRKY domain[18,44], thus activating the RRS1-R/RPS4 complex when transgenically expressed in Arabidopsis Col-0 plants. Crossing *RAREOE* into the transgenic plants expressing RRS1-R^{slh1} and RRS1-R^{T1214A} rescued their autoimmune phenotypes, including dwarfism and elevated *Pathogenesis-related Proteins 1* (*PR1*) and *PR2* expression (Fig. 4E–F). The endogenous RRS1/RPS4 complex confers resistance against bacterial pathogen *Pst* DC3000(AvrRps4) in wild-type plants. Compared to wild-type plants, the *RAREOE* plants exhibited compromised resistance, while the *rare* mutants displayed enhanced resistance (Fig. 4G). Taken together, these data suggest RARE negatively regulates HR and resistance-mediated by the RRS1/RPS4 complex.

To verify that the diminished RRS1 accumulation accounts for impaired RRS1/RPS4-mediated immunity in the *RAREOE* plants, we crossed the *RAREOE* lines with FLAG-tagged *RRS1-R* transgenic line #4 with higher RRS1-R protein levels (Supplementary Fig. 10D). This largely restored resistance to *Pst* DC3000 carrying AvrRps4 in the *RAREOE* plants(Fig. 4H), indicating that the susceptibility of the *RAREOE* lines was caused by diminished RRS1 accumulation. Taken together, our data indicate that RARE destabilizes the RRS1/RPS4 complex by promoting RRS1 degradation, thus compromising RRS1/RPS4-mediated defense responses.

UBP12/UBP13 counteract RARE's regulation of RRS1/RPS4 complex

Deubiquitinating enzymes (DUBs) remove ubiquitin from ubiquitinated substrates, reversing the ubiquitination process. The Arabidopsis ubiquitin-specific proteases (UBPs) belong to the largest subfamily of DUBs and regulate diverse cellular processes[45,46]. Like E3 ligase RARE, UBP12 and UBP13, two functionally redundant UBPs[35], were identified in the proximal proteome of RRS1-R (Supplementary Data 1). Co-IP and pull-down assays showed that UBP12/UBP13 target RRS1/RPS4 complex through directly binding the WRKY domain of RRS1 (Supplementary Fig. 11A-C). We therefore tested if they counteract RARE's regulation of RRS1/RPS4. Semi-in vitro deubiquitination assays revealed that immunoprecipitated RRS1 from the *pAT2::RRS1-R-FLAG* plants was deubiquitinated by UBP12 and UBP13, but not their deubiquitinase-dead variants UBP12^{C208S} and UBP13^{C207S}(Fig. 5A). Neither UBP12 nor UBP13 affected autoubiquitination of RARE (Supplementary Fig. 12A). These data indicate that UBP12 and UBP13 directly deubiquitinate RRS1 in a deubiquitinase activity-dependent manner without affecting RARE's activity. RARE ubiquitinates RRS1 on its integrated WRKY domain. We next examined if UBP12/UBP13 can remove RARE-catalyzed ubiquitination of RRS1-R^{WRKY}. The ubiquitinated RRS1-R^{WRKY}, generated through in vitro ubiquitination reaction with RARE and subsequently purified, was dramatically reduced by adding UBP12 or UBP13, but not their deubiquitinase-dead variants nor the negative control UBP7 (Fig. 5B, Supplementary Fig. 12B), as revealed by the in vitro deubiquitination assays. These results demonstrate that UBP12/UBP13 antagonize RARE-mediated ubiquitination of RRS1-R^{WRKY}.

https://doi.org/10.1038/s41467-025-57231-9

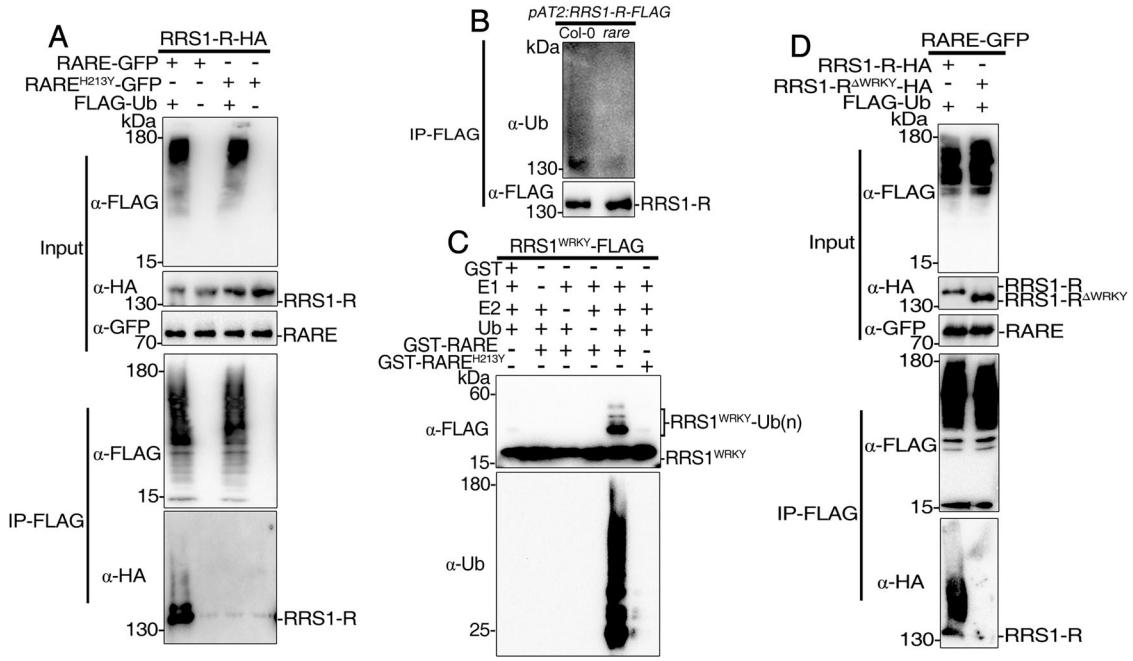

Fig. 3 | RARE ubiquitinates RRS1 through its integrated WRKY domain. **A** Detection of ubiquitination of RRS1-R by RARE in *Nb* leaves. HA-tagged RRS1-R was co-expressed with GFP-tagged RARE or its mutant form RARE (H213Y) in the presence or absence of FLAG-Ub in *Nb* leaves. The *Nb* leaves were pretreated with 50 μM MG132 for 6 h before harvesting. Total ubiquitinated proteins were immunoprecipitated at 36 h post-infiltration with anti-FLAG antibody, and ubiquitinated RRS1-R proteins were detected by immunoblotting with anti-HA antibody. **B** Reduced in vivo ubiquitination level of RRS1 in *rare* mutant compared to wild-type background. Total protein extracts from FLAG-tagged RRS1 plants in wild-type or *rare* background were subjected to immunoprecipitation using anti-FLAG antibody. Following immunoprecipitation with anti-FLAG antibody, the ubiquitination of RRS1 was detected by immunoblot analysis using anti-Ubiquitin antibody. Immunoblots were probed with anti-ubiquitin and anti-FLAG antibody, respectively. **C** Ubiquitination of WRKY domain of RRS1 by RARE in vitro. FLAG-tagged WRKY domain of RRS1 was incubated with GST-RARE in ubiquitination assay buffer. Samples were resolved by SDS-PAGE and subjected to immunoblot analysis with anti-FLAG (top panel) or anti-Ub (bottom panel) antibody. Direct ubiquitination of WRKY domain was evident by higher molecular laddering detected by immunoblotting with anti-FLAG antibody. **D** WRKY domain is required for RRS1 ubiquitination by RARE. HA-tagged RRS1-R or its WRKY domain deletion variant was co-expressed with GFP-tagged RARE in the presence of FLAG-Ub in *Nb* leaves. The *Nb* leaves were pretreated with 50 μM MG132 for 6 h before harvesting. Total ubiquitinated proteins were immunoprecipitated at 36 h post-infiltration with anti-FLAG antibody, and ubiquitinated RRS1-R proteins were detected by immunoblotting with anti-HA antibody.

To investigate the deubiquitination of RRS1 by UBP12/UBP13 in vivo, the *pAT2::RRS1-R-FLAG* transgene was crossed into *UBP12OE*, *UBP13OE* transgenic lines and *ubp12-2w*, a weak double mutant with reduced *UBP12* and *UBP13* transcripts, since the *ubp12ubp13* double null mutants are infertile[47]. Polyubiquitinated RRS1-R levels were greatly increased in *ubp12-2w* and reduced in *UBP12OE* and *UBP13OE* compared to those in wild-type (Figs. 5C and Supplementary Fig. 13A). To correlate UBP12/UBP13 with RRS1 abundance, we compared RRS1 protein abundance in these backgrounds. RRS1 accumulation was significantly increased in *UBP12O*E and *UBP13OE* but reduced in *ubp12-2w* background (Fig. 5D). The addition of MG132 partially restored RRS1 abundance in *ubp12-2w* (Supplementary Fig. 13B). Consistently, UBP12 and UPB13 rescued the RARE-mediated reduction of RRS1-R and RPS4 in a deubiquitinase activity-dependent manner (Fig. 5E). Collectively, these results suggest that UBP12 and UBP13 deubiquitinate RRS1, protecting it from proteasomal degradation and thereby stabilizing the RRS1/RPS4 complex.

Finally, we tested whether UBP12/UBP13 affect RRS1/RPS4-mediated immune responses. HR assay in tobacco showed that UBP12/UBP13, but not their mutants, alleviated RARE-mediated suppression of HR triggered by RRS1-R/RPS4 in recognition of AvrRps4 (Fig. 5F). Additionally, introducing *UBP12OE* and *UBP13OE* into the *RAREOE* lines by crossing partially rescued the enhanced susceptibility of the *RAREOE* lines against *Pst* DC3000(AvrRps4) (Fig. 5G). These results indicate that UBP12/UBP13 counteract RARE's inhibition of RRS1/RPS4-mediated immune responses. Taken together, our data suggest that UBP12 and UBP13 antagonize RARE-mediated ubiquitination of RRS1-R, consequently protecting the accumulation and defense responses of the RRS1/RPS4 complex.

RARE and UBP12/UBP13 antagonistically regulate two WRKY transcription factors homologous to RRS1^{WRKY}

IDs, usually homologous to effector target proteins, were incorporated into NLR-IDs through domain shuffling for effector detection during evolution[24]. Phylogenetic analysis revealed that RARE and UBP12/UBP13 are both conserved across monocots and dicots (Supplementary Fig. 14A, B). In contrast, RRS1 homologs carrying the integrated WRKY domain are limited to the Camelineae tribe. Outside of this tribe, RRS1 homologs lack the WRKY ID (Fig. 6A), suggesting that WRKY domain integration likely occurred during the diversification of Camelineae tribe within the Brassicaceae family. RARE and UBP12/UBP13 antagonistically regulate the reversible ubiquitination of RRS1 through ubiquitinating/deubiquitinating the WRKY ID. Given the limited co-existence of RARE and UBP12/UBP13 with RRS1-R^{WRKY} domain during evolution, the initial roles of RARE and UBP12/UBP13 may be involved in homeostatic regulation of effector targets homologous to RRS1-R^{WRKY}.

Our previous studies show that WRKY70, WRKY41 and WRKY33 are three putative targets of AvrRps4 and PopP2[16]. The WRKY domains of WRKY70 and WRKY41, but not WRKY33, are in the same clade as RRS1-R^{WRKY} in the phylogenetic tree (Supplementary Fig. 14C), suggesting that they are homologous to RRS1-R^{WRKY}. Consistent with our speculation, ubiquitination assays showed that RARE is capable of ubiquitinating the WRKY domains and full-length of

https://doi.org/10.1038/s41467-025-57231-9

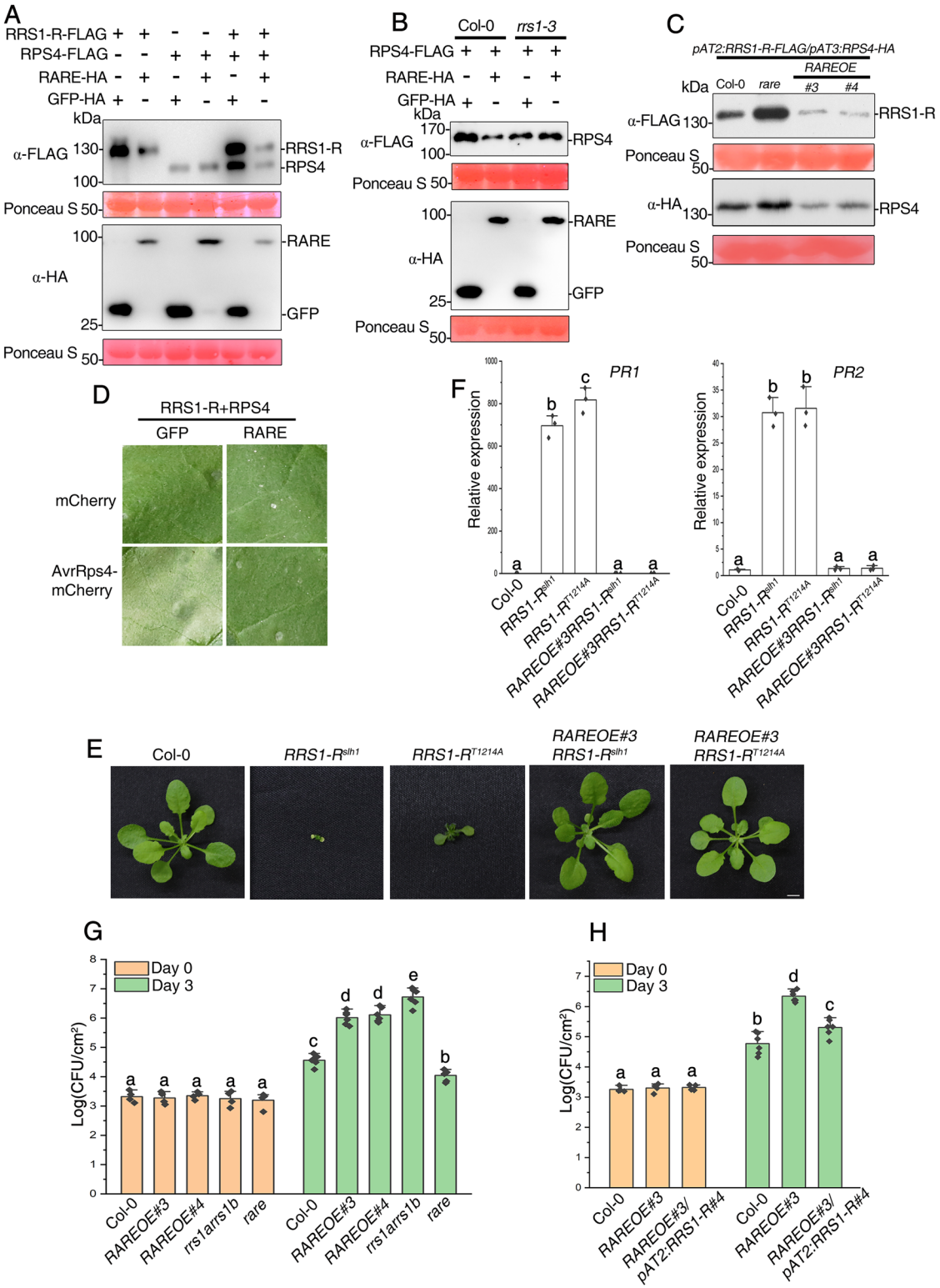

WRKY70, WRKY41 but not WRKY33 (Fig. 6B, C). As expected, UBP12 and UBP13 also can remove ubiquitin from ubiquitinated WRKY domains of WRKY41 and WRKY70 catalyzed by RARE (Figs. 6D, Supplementary Fig. 15A). These data suggest that WRKY70 and WRKY41 are under reversible ubiquitination regulation by RARE and UBP12/UBP13. Consistent with UBP12/UBP13 regulating the ubiquitination of WRKY41 and WRKY70 in a manner opposite to RARE, RARE promoted the degradation of WRKY70 and WRKY41, but not WRKY33, while UBP12/UBP13 inhibited such degradation (Figs. 6E, Supplementary Fig. 15B, C), indicating antagonistic control of WRKY70 and WRKY41 stability.

In addition, we found that the *rare* mutants exhibit enhanced basal resistance against *Pst* DC3000, while the *RAREOE* lines show reduced resistance (Supplementary Fig. 16). The suppression of basal resistance by RARE is likely through its destabilization of WRKY70 and WRKY41, two positive regulators of basal resistance[48,49]. Silencing of UBP12/UBP13 enhanced resistance against *Pst* DC3000[35], which seems contradictory to the stabilization of WRKY70 and WRKY41 by UBP12/

Fig. 4 | RARE destabilizes RRS1/RPS4 complex in a RRS1-dependent manner and negatively regulates RRS1/RPS4–mediated defense responses. A RARE directly destabilizes RRS1 and indirectly destabilizes RPS4 in the presence of RRS1. RRS1-R, RPS4 or RRS1-R/RPS4 were transiently co-expressed with RARE in *Nb* at 2 dpi and then subjected to immunoblotting with anti-FLAG antibody for detecting RRS1-R/RPS4 or anti-HA antibody for detecting RARE. The HA-tagged GFP served as a control. **B** RARE modulates RPS4 homeostasis via RRS1. RPS4-FLAG was co-expressed together with RARE-HA or GFP-HA in protoplasts from Col-0 or *rrs-1* plants. RPS4-FLAG proteins were detected by immunoblotting with anti-FLAG antibody. **C** Immunoblot analyses of RRS1-R and RPS4 protein levels in Col-0, *rare*, and *RAREOE* background. Total proteins were extracted from 10-days-old seedlings and subjected to immunoblotting using anti-FLAG antibody for detecting RRS1-R and anti-HA antibody for detecting RPS4, respectively. Ponceau S staining of Rubisco indicates equal loading. **D** Suppression of RRS1/RPS4-mediated cell death upon AvrRps4 perception in tobacco plants. Each leaf section was transiently coinfiltrated with RRS1-R/RPS4, AvrRps4, and either GFP or RARE. Photographs assessing HR were taken 4 dpi. **E** Overexpression of RARE suppresses the auto-immune phenotype triggered by RRS1-R^{slh1} and RRS1-R^{T1214A}, the auto-active alleles of RRS1-R. Morphology of 5-week-old soil-grown plants of Col-0, *RRS1-R^{slh1}*, *RRS1-R^{T1214A}*, *RAREOERRS1-R^{slh1}* and *RAREOERRS1-R^{T1214A}*. Scale bar, 0.5 cm. **F** Relative expression levels of *PR1* and *PR2* were determined by real-time PCR. The relative transcript levels of *PR1* and *PR2* were normalized to the expression of *UBQ*. Data are shown as means ± SD (n = 3 biological replicates). **G** *RAREOE* lines are compromised in RRS1/RPS4-mediated resistance against *Pst* DC3000(AvrRps4). 5-week-old plants were infiltrated with the bacteria at OD_{600} = 0.0005. Leaf disks within the infiltrated area were taken at days 0 and 3 to measure the bacterial growth. **H** Introduction of the *RRS1-R* transgene into the *RAREOE#3* line restores disease resistance to *Pst* DC3000(AvrRps4). Note that the epitope-tagged RRS1-R/RPS4 transgenic line#4 was used to cross with *RAREOE* transgenic line. For (**G**–**H**), data are shown as means ± SD (n = 4 and 6 biological replicates, respectively). For (**F**–**H**), the corresponding p values can be found in the Source Data.

UBP13. The paradox likely arises from the compound effects of UBP12/UBP13 substrates functioning as negative regulators of basal resistance, including MYC2, NPR3 and NPR4, that are also stabilized by UBP12/UBP13[45,50]. Collectively, these results suggest that RARE and UBP12/UBP13 antagonistically regulate ubiquitination and stability of WRKY70 and WRKY41, which carry homologous WRKY domains to RRS1, and that such regulatory mechanism was co-opted to modulate RRS1/RPS4 complex homeostasis during WRKY domain integration into RRS1(Fig. 6F). Therefore, WRKY ID-mediated ubiquitination of RRS1 has been retained in evolution and continues to contribute for fine-tuning homeostasis of RRS1/RPS4 complex.

Discussion

NLR homeostasis must be tightly regulated to ensure proper defense without triggering autoimmunity. Many NLRs have been shown to associate with diverse group of NLR-interacting proteins to achieve initiation and fine-tuning of immune responses, which forms another layer of regulation of NLR activity. In this study, we exploited TurboID-based proximity labeling proteomics to profile the proxiomes of RRS1/RPS4 complex using RRS1-R-TurboID transgenic plants. A number of regulators potentially involved in the RRS1/RPS4-mediated immune response were identified. Some proteins that have been previously reported to be associated with other NLRs or to participate in the immune signaling, such as TPR proteins, MAC1 and MAC5A, were also identified in our dataset[32,33]. So far, no interacting partner has been identified to modulate the activity or stability of RRS1/RPS4 complex. Therefore, the proteomic datasets described in this work provide an overview of regulatory proteins and signaling partners associated with RPS4/RRS1 complex, thus enhancing our understanding of the dynamic and intricate regulatory network during NLR-mediated immunity.

Unlike singleton NLRs, RRS1 and RPS4 form two-component immune complex that has been developed as a model for molecular understanding of paired NLR protein mechanisms. Despite its importance, the molecular mechanism involved in the control of complex formation and regulation remain poorly understood. In this complex, our previous studies revealed that RRS1 acts as a platform that enables the proper assembly of a functional RRS1/RPS4 complex and enhances the protein accumulation of RPS4[42,43]. Here, we revealed a reversible ubiquitination cycle in which the deubiquitinases UBP12 and UBP13 integrate with the E3 ligase RARE to coordinately modulate the complex turnover through (de)ubiquitinating the WRKY ID of RRS1. RARE directly interacts and ubiquitinates the integrated WRKY domain of RRS1, facilitating its proteasomal degradation. Since RRS1 stabilizes RPS4, RARE destabilization of RRS1 subsequently reduces RPS4 accumulation. Therefore, RARE impairs the complex abundance by promoting RRS1 and RPS4 degradation directly and indirectly, respectively.

Several studies have shown the dynamic homeostasis regulation of NLRs in inactive and active states[51,52]. In our study, we found that AvrRps4 perception dramatically enhances RRS1 protein abundance and impairs its ubiquitination, most likely due to the weakened interaction between RRS1 and RARE upon AvrRps4 recognition (Supplementary Figs.17 A–C). Moreover, AvrRps4-triggered ETI induces the protein accumulation of UBP12/UBP13 although their association with RRS1 remains almost unaffected(Supplementary Figs.17 D, E), further analysis of publicly available transcriptome data revealed that transcription of UBP12/UBP13 is induced while RARE transcription is suppressed following inoculation of *Pseudomonas fluorescens 0–1 (Pf0-1)* carrying AvrRps4 (Supplementary Fig.17F). These results suggest that AvrRps4 recognition could induce UBP12/UBP13 accumulation but inhibit the accumulation of RARE as well as its association with RRS1. Based on the findings, we speculate that RARE ubiquitinates and promotes the degradation of RRS1 through the 26S proteasome pathway to keep the RRS1/RPS4 complex at a low level in the resting state. When ETI is activated through the recognition of AvrRps4 by the RRS1/RPS4 complex, the protein abundance of UBP12/UBP13 is increased, and increased UBP12/UBP13 subsequently counteract RARE's action, thereby preventing the degradation of RRS1 under active state and safeguarding the complex. As a consequence, the active state of RRS1/RPS4 complex is stabilized and accumulates to a sufficient level to induce a robust ETI response. Our study reveals the delicate, reversible ubiquitination control of paired NLR complex levels that fine-tunes immunity, advancing understanding of paired NLR complex homeostatic regulation.

We further demonstrate that reversible ubiquitination regulates WRKY70/WRKY41, which are putative virulence targets of AvrRps4 and PopP2 and homologous to the WRKY ID of RRS1, through the action of RARE and UBP12/UBP13. Critically, we show this post-translational regulatory mechanism likely transfers from the WRKY proteins to the NLR-ID protein RRS1-R via integration of the WRKY domain, enabling homeostatic modulation of RRS1/RPS4-mediated immunity. Such evolutionary jumps likely synchronize the RRS1/RPS4 abundance with the WRKY70/WRKY41 levels, and possibly more other WRKY transcription factors. This aligns with the emerging view of unified plant immune system and concerted action of two sets of immune receptors since WRKY transcription factors are downstream components of PRRs required for basal immunity[48,49,53–56].

Our finding of the transfer of reversible ubiquitination from WRKY70/WRKY41 to RRS1 through WRKY domain integration exposes an underexplored phenomenon with profound implications for protein regulation. It raises questions about the prevalence of this phenomenon and its impact on expanding organismal post-translational modification (PTM) regulatory network. Various extraneous domains like WRKY, zinc-finger BED and kinase domains have repeatedly integrated into NLR proteins across all plant lineages[8,9]. Non-integrated

https://doi.org/10.1038/s41467-025-57231-9

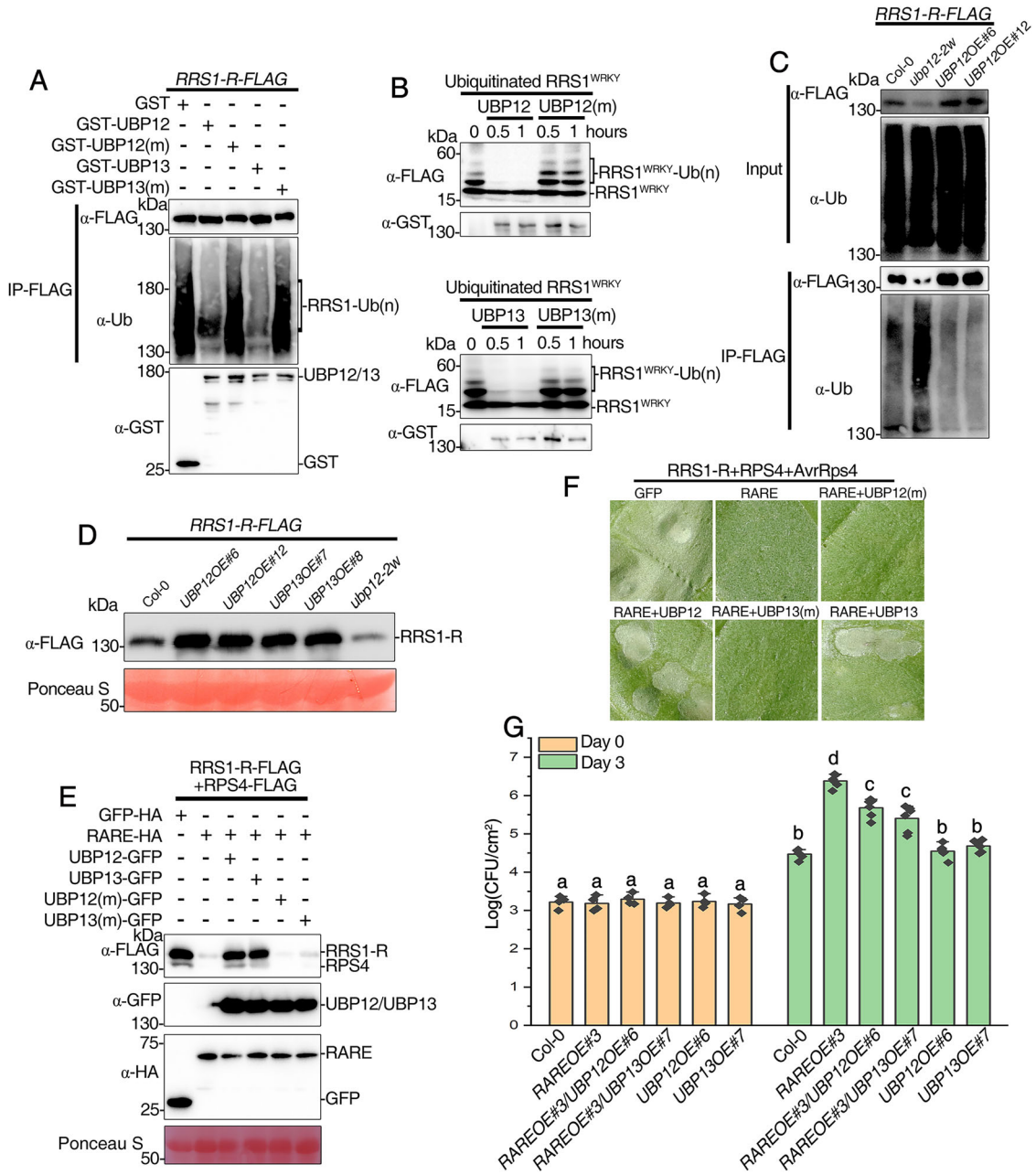

Fig. 5 | UBP12 and UBP13 counteract the effect of RARE by removing ubiquitin from polyquibiquinated RRS1. A Deubiquitination of RRS1 expressed in Arabidopsis plants by recombinant UBP12/UBP13. Polyubiquitinated RRS1 proteins were immunoprecipitated with agarose-conjugated anti-FLAG antibody from 10-day-old seedlings and subsequently co-incubated with GST-UBP12/UBP13 or GST-UBP12^{C208S}/UBP13^{C207S}. Immunoprecipitated RRS1 was detected by anti-FLAG antibody (top panel). RRS1 ubiquitination status was analyzed by immunoblotting with anti-ubiquitin antibody (middle panel). The presence of UBP proteins was confirmed by the anti-GST antibody (bottom panel). **B** UBP12/UBP13 deubiquitinate polyubiquitinated WRKY domain of RRS1 in vitro. Polyubiquitinated WRKY domain proteins produced by ubiquitination in the presence of E1(UBA2), E2 (UBC10), RARE and ubiquitin (Ub) were pulled down and then incubated with GST-UBP12/UBP13, or their catalytically inactive variants for 0.5 or 1 hour. Ubiquitinated WRKY domain was detected by anti-FLAG antibody (top panel). GST-tagged UBP proteins were detected with anti-GST antibody (bottom panel). **C** The polyubiquitination status of RRS1 in various genotypes. 10-days-old seedlings grown on MS medium were pretreated with 50 mM MG132 for 6 h. Protein extracts were immunoprecipitated with agarose-conjugated anti-FLAG antibody, followed by immunoblotting with anti-FLAG (top panel) and anti-ubiquitin antibody (bottom panel). **D** The protein levels of FLAG-tagged RRS1 driven by pAT2 promoter in various genotypes. Total protein extracts were subjected to immunoblotting with anti-FLAG antibody for detecting RRS1-R. Two independent lines were used in (**C**) and (**D**) separately. **E** UBP12/UBP13 antagonize RARE-mediated RRS1/RPS4 complex degradation. RRS1/RPS4 was co-expressed with RARE in *Nb* leaves in the presence or absence of UBP12/UBP13. GFP was coexpressed as a control. **F** UBP12/UBP13 attenuate RARE-mediated suppression of cell death caused by coexpression of RRS1-R/RPS4 and AvrRps4. Each leaf section was transiently coinfiltrated with RRS1-R/RPS4, AvrRps4, and the indicated construct(s). Photographs assessing HR were taken 4 dpi. **G** Bacterial growth of *Pst* DC3000(AvrRps4) on 5-week-old leaves of the indicated genotypes at 0 and 3 dpi with bacterial inoculum of $OD_{600} = 0.0005$. Statistical significance is indicated by different letters ($P < 0.01$, one-way ANOVA followed by Tukey's post hoc test). Data are shown as means ± SD ($n = 4$ and 6 biological replicates, respectively). The corresponding p values can be found in the Source Data.

https://doi.org/10.1038/s41467-025-57231-9

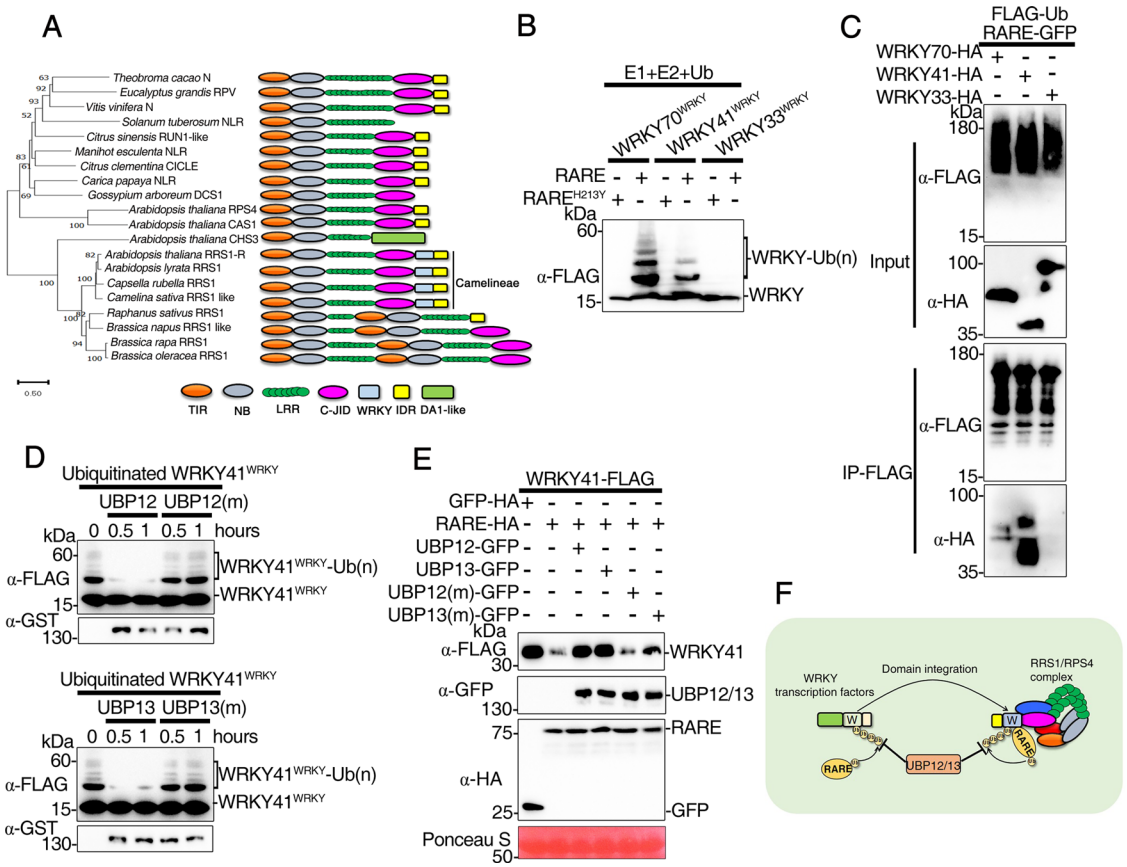

Fig. 6 | RARE and UBP12/UBP13 antagonistically regulate the stability some WRKY transcription factors homologous to RRS1^{WRKY}. A The phylogenetic tree of RRS1 orthologues (left) and their domain architecture (right). The tree was generated using the neighbor-joining method based on full-length amino acid sequences. Only bootstrap values > 50% within 1000 replicates are shown above branches. RPS4, CSA1 and CHS3 serve as outgroup. **B** RARE ubiquitinates the WRKY domain of WRKY70, WRKY41 but not WRKY33. FLAG-tagged WRKY domains were incubated with GST-RARE or its mutant form RARE (H213Y) in ubiquitination assay buffer containing E1(UBA2), E2 (UBC10) and Ub. Samples were resolved by SDS-PAGE and subjected to immunoblot analysis with anti-FLAG antibody for detecting higher molecular weight laddering bands. **C** Detection of ubiquitination of WRKY70 and WRKY41 but not WRKY33 by RARE in *Nb* leaves. HA-tagged WRKY proteins were co-expressed with GFP-tagged RARE in the presence of FLAG-Ub in *Nb* leaves. The *Nb* leaves were pretreated with 50 μM MG132 for 6 h before harvesting. Total ubiquitinated proteins were immunoprecipitated at 36 h post-infiltration with anti-FLAG antibody, and ubiquitinated WRKY proteins were detected by immunoblotting with anti-HA antibody. **D** UBP12 and UBP13 deubiquitinate polyubiquitinated WRKY domain of WRKY41 in vitro. Polyubiquitinated WRKY domain proteins produced by ubiquitination in the presence of E1(UBA2), E2 (UBC10), RARE and ubiquitin (Ub) were pulled down and then incubated with GST-UBP12, GST-UBP13, or their catalytically inactive variants for 0.5 or 1 hour. Ubiquitinated WRKY domain was detected by anti-FLAG (top panel). GST-UBP12, GST-UBP13 or the inactive variants were detected with anti-GST antibody (bottom panel). **E** UBP12/UBP13 antagonize RARE-mediated WRKY41 degradation. WRKY41 was co-expressed with RARE in *Nb* leaves in the presence or absence of UBP12/UBP13. GFP was coexpressed in the experiment as a control. **F** A model illustrating UBP12/UBP13- and RARE-mediated (de)ubiquitinating the WRKY ID of RRS1 as an evolutionarily gained modification for fine-tuning homeostasis of RRS1/RPS4 complex.

proteins harboring these homologous domains can undergo different types of PTMs such as phosphorylation, sumoylation or acetylation, suggesting the potential transfer of these modifications to regulate NLR-IDs' function after domain integration, thus endowing NLR-ID fusion proteins with an additional layer of regulatory features. Similarly, the Src homology 2 (SH2) domain, a phosphotyrosine-binding domain indispensable for the receptor tyrosine kinase signaling pathways, represents another potential case of PTM transfer through domain shuffling. Rapid evolution of phosphotyrosine signaling by shuffling SH2 domains into various proteins with a range of biochemical properties including catalytic kinase domain endows SH2 domain with phospho-regulation by the Src family kinases[57,58], echoing our findings.

In summary, our results are complementary to the previous work reporting RRS1/RPS4 complex is subjected to multilayered regulation, including phosphorylation, transcriptional regulation and alternative splicing[18,59,60]. This study has revealed a new layer of post-translational regulation by ubiquitination and deubiquitination of the ID of RRS1. The countering activities of RARE and UBP12/UBP13 antagonistically and dynamically control the turnover of RRS1/RPS4 complex to maintain immune homeostasis. Since the molecular mechanism of paired NLR protein complex regulation remains largely unknown, our study not only provides a mechanism for regulating paired NLR/NLR-ID complex homeostasis, but also presents an example in which transfer of PTMs through domain integration, which allows the emergence of novel post-translational regulatory circuitries.

Methods

Plant materials and growth conditions

The wild-type *Arabidopsis thaliana* plants used in this study were the Columbia-0 (Col-0). The mutant *ubp12-2w* (GABI_742C10) seeds were provided by Dr. Xia. Cui (Chinese Academy of Agricultural Sciences, Beijing, China) and these mutants have been described by Cui et al.[47]. The *rare* mutant line (SALK_093498C) was ordered from the Arabidopsis Biological Resource Center (ABRC, Ohio State University, USA). *rrs1arrs1b* and *rrs1-3* (SALK_061602) have been described by Saucet SB,

et al.[29]. Arabidopsis plants were grown in a growth room at 22 °C under a 14 h light/10 h dark photoperiod with light density of 100 µmol m^{-2} s^{-1}. *Nicotiana benthamiana* (*Nb*) and *Nicotiana tabacum* (cultivar 'Petite Gerard') plants were grown at 24 °C under long-day photoperiod (16 hr light/8 hr dark) with light density of 120 µmol m^{-2} s^{-1}. Leaves of four- to five-week-old plants were used for *Agrobacterium*-mediated transient expression assays.

Plasmid construction and generation of transgenic plants

Plasmids were constructed using Golden Gate cloning as previously described[17]. Briefly, to clone the full-length gene or individual fragment with different tags, all the full-length "domesticated" coding sequence (removal of internal BsaI/BbsI sites without change the encoded amino acid) gene/fragment without stop codon were cloned into the coding sequencing module level 0 vector (pICSL01005). The resulting constructs were assembled with different C-terminus tags into level 1 binary vector pICSL86977 with the CaMV35S promoter, Ocs terminator C-terminal epitope tags. For generation of N-terminal epitope tagging vector, the resulting constructs were assembled with different N-terminus tags into level 1 binary vector pICSL86900 with the CaMV35S promoter, Ocs terminator and N-terminal epitope tags. The C-terminus tags used in this study include C-TurboID(pICSL50040), C-3xFlag (pICSL50007), C-HA (pICSL50009), C-Myc (pICSL50010), C-GFP (pICSL50008), cYFP(pICSL50002) and nYFP(pICSL50003). The N-terminus tag used in this study includes N-Flag (pICSL30005). The primers used in this study are listed in Supplementary Table 1. For generation of transgenic plants, constructs were introduced into *Agrobacterium* strain GV3101 and subsequently transform Arabidopsis using the floral dip method. The harvested seeds from transformed Arabidopsis were resuspended in 0.1% agarose and detection of transgenic seeds using red fluorescent protein (DsRed) as a visible marker. Positive transformants were selected based on the seeds with bright red fluorescence under a hand-held lamp LUYOR-3415RG (Luyor Instrument, Shanghai).

Protein extraction, immunoblot analysis and Co-IP assay

For Co-IP assays in *Nb* leaves was performed as previously described with minor modifications[18], *Nb* leaves were harvested 48 h post agroinfiltratiion and ground in liquid nitrogen to a fine powder using a pestle and mortar. The powder was subsequently homogenized in an equal volume of ice-cold GTEN buffer (10% glycerol, 150 mM Tris-HCl pH 7.5, 1 mM EDTA, 150 mM NaCl) supplemented with 10 mM DTT, 0.2% (vol/vol) Nodinet-40, Anti-protease tablet (Complete EDTA-free Roche) and 2% PVPP (Polyvinylpolypyrrolidone) on a rotator for 20 min at 4 °C. The lysates were then centrifuged at 5000 g for 30 min at 4 °C, and the supernatant was filtered through 0.45 mm filters. The filtered protein extract was mixed with 3xSDS loading buffer (30% glycerol, 3.3% SDS, 94 mM Tris-HCl pH 6.8, 0.05% (vol/vol) bromophenol blue) supplemented with 10 mM DTT for input samples or for immunoblot analysis. Immunoprecipitations were performed using filtered extract incubated with Anti-DYKDDDDK G1 Affinity Resin (GenScript, L00432) or Anti-HA IP Resin (GenScript, L00777) at 4 °C for 2 h with gentle shaking. After incubation, beads were collected via centrifugation at 7000 rpm for 30 seconds, washed three times in washing buffer (GTEN buffer supplemented with 10 mM DTT, 0.2% Nodinet-40 and Anti-protease tablet) and then suspended in 2XSDS loading buffer containing 10 mM DTT before boiling at 95 °C for 5 min.

For Co-IP assays performed in Arabidopsis protoplasts, protoplasts co-transfected with the indicated plasmids were harvested after overnight incubation at 23 °C and lysed with native extraction buffer (150 mM Tris-HCl, pH 7.5, 0.5% Nonidet P-40, 2 mM EDTA, 150 mM NaCl, 10% glycerol, 1 mM $NaVO_3$, 5 mM NaF and 1Xprotease inhibitor cocktail (Roche)) by vigorous vortexing for 1 min. The lysates were centrifuged at 12,000 g for 10 min at 4 °C and supernatant was incubated with Anti-HA IP Resin for 2 h at 4 °C with gentle mixing. The antibody-coupled agarose beads were collected and washed three times using native extraction buffer. The precipitated beads were then resuspended in 30 µL of 2X SDS loading buffer denatured for 10 min at 96 °C.

The co-immunooprecipated proteins were electrophoretically separated by SDS-PAGE and then transferred to Immobilon-P PVDF membranes (Merck Millipore) using a wet transfer apparatus (Bio-Rad). After blocking at room temperature for 1 h with 5% nonfat dry milk in 1×Tris-buffered saline containing 0.1% Tween 20, membrane was incubated with Horseradish Peroxidate (HRP) conjugated antibodies (Anti-FLAG M2, 1:10000 dilution, Sigma; Anti-GFP, 1:10000 dilution, Santa Cruz Biotechnology) in TBST supplemented with 5% milk by gentle agitation at room temperature for 1 h. The membrane was then washed 3 times with agitation for 5 min in TBST, and once in TBS (Tris-Buffered Saline). Proteins of interest were visualized by luminescence of HRP using the chemiluminescent substrate on a Tanon-5200 Chemiluminescent Imaging System (Tanon Science and Technology).

Expression of recombinant protein, in vitro ubiquitination and deubiquitination assays

Constructs of GST- and HA-tagged RARE, GST-tagged UBP12/UBP12 (m), GST-tagged UBP13/UBP13 (m), His-and FLAG-tagged $RRS1^{WRKY}$, His-and FLAG-tagged $RRS1B^{WRKY}$, His-and FLAG-tagged $WRKY70^{WRKY}$/$WRKY41^{WRKY}$/$WRKY33^{WRKY}$ were introduced into and expressed in *Escherichia coli* Transetta(DE3) for purification following the manufacturer's instructions. The in vitro ubiquitination/deubiquitination assays were conducted following the procedure previously described[45,61]. Briefly, 2 µg ubiquitin, 50 ng AtUBA2, 100 ng AtUBC10, 500 ng RARE, and with or without 500 ng substrate proteins were added to 30 µl ubiquitination buffer (50 mM Tris-HCl, pH 7.5, 5 mM $MgCl_2$, 2 mM ATP and 2 mM dithiothreitol). Reactions were incubated at 30 °C for 2 h and the reaction mixtures were subsequently separated on SDS-PAGE followed by immunoblot analysis using anti-Ub, anti-FLAG, or anti-GST antibody, respectively. For in vitro deubiquitination, after incubation with E1, E2 and E3 for 2 h at 30 °C, polyubiquitinated substrates proteins were purified and then added to deubiquitination buffer (50 mM Tris-HCl, pH 7.4, 150 mM NaCl, 5 mM $MgCl_2$, and 2 mM DTT) followed by the addition of GST-UBP12, GST-UBP12(m), GST-UBP13 or GST-UBP13(m). The deubiquitination reactions were terminated by adding 4XSDS loading buffer. The samples were taken at 0.5 and 1 h and subjected to immunoblot analysis using anti-Ub, anti-FLAG, or anti-GST antibody, respectively.

Bacterial growth assay

P. syringae pv. *tomato* DC3000(AvrRps4) or *P. syringae* pv. *tomato* DC3000 were grown on selective King's B (KB) medium plates overnight. Bacterial cells were harvested, washed and resuspended in 10 mM $MgCl_2$ at a concentration of $OD_{600} = 0.0005$ for infiltration. Leaves of five-week-old Arabidopsis were hand-infiltrated using a 1 mL needleless syringe. The infected leaves are harvested at 0 and 3 days post inoculation to quantify bacterial colonies. 2 leaf disks from one plant (one leaf disc per leaf) were collected and were ground in 10 mM $MgCl_2$, serially diluted, spotted on selective LB agar plates. The plates were incubated at 28 °C for two days before counting.

Subcellular localization, BiFC assay and confocal laser-scanning microscopy

BiFC analysis was performed in transient transfection assays as previously described[62]. The combinations of plasmids containing N- and C-terminal YFP fusions were co-transformed into Arabidopsis protoplasts using PEG-calcium-mediated transformation. The transfected protoplasts were incubated overnight under dim light at 23 °C before observation. Images were captured using a Leica TCS SP5 confocal fluorescence microscope. For GFP fluorescence, the excitation

wavelength was 488 nm and the emission spectra were collected at 495 to 525 nm, respectively. For DAPI fluorescence, the excitation wavelength was 358 nm and the emission spectra were collected at 415 to 515 nm, respectively. For chlorophyll autofluorescence, the excitation wavelength was 488 nm and emission spectra were collected at 650 to 750 nm, respectively.

RNA extraction and quantitative reverse transcription-PCR (qRT-PCR)

Total RNA was extracted from 3-week-old plants using TRIzol reagent and then treated with DNase I to remove DNA contamination. Reverse transcription was conducted using PrimeScript II 1st Strand cDNA Synthesis Kit (Takara) following manufacturer's protocol. Quantitative RT-PCR were performed in the ABI QuantStudio 6 Flex Real-Time PCR System using the SYBR Premix ExTaq kit (Takara) in accordance with the manufacturer's instructions. Three biological replicates were performed for each sample, and the expression levels were normalized to those of *UBQ10* using the comparative $2^{-\Delta\Delta Ct}$ method. Primers used for real-time PCR were listed in Supplementary Table 1.

Proximity biotinylation, free biotin depletion and affinity purification by streptavidin-coated beads

One-week-old transgenic seedlings expressing TurboID-tagged bait proteins (0.4 g) were soaked in 50 µM biotin solution for 3 h and quickly washed three times with ice cold water to stop labeling reaction and to deplete excess biotin. The seedlings were then dried with paper towels and subsequently ground into fine powder with liquid nitrogen. The sample powder was resuspended with protein extraction buffer (150 mM Tris-HCl, pH 7.5, 150 mM NaCl, 0.5% Triton X-100, 0.5% Nonidet P-40, 0.5% sodium deoxycholate, Anti-protease tablet (Complete EDTA-free Roche)) with gentle mixing and then centrifuged at 12,000 g for 10 min. The resulting supernatant was then run through the Zeba™ Spin Desalting Column (Thermo Fisher Scientific, Catalog number 89893) according to manufacturer's instruction to remove the excess biotin in lysates. The elution was then mixed with 50 µL of the equilibrated streptavidin agarose beads (Catalog number 20349, Thermo Fisher Scientific) and incubated overnight at 4 °C. The beads were subsequently washed 3 times with washing buffer (150 mM Tris-HCl, pH 7.5, 150 mM NaCl, 0.5% Nonidet P-40, Anti-protease tablet (Complete EDTA-free Roche)) and transferred to new low protein binding tube (Thermo Fisher Scientific). The biotinylated proteins were eluted by 30 µL 2×SDS sample buffer and detected by immunoblot analysis using streptavidin-HRP (Catalog Number. N100, Thermo Fisher Scientific).

Phylogenetic analysis

To avoid long-branch attraction, the neighbor-joining method, rather than the maximum likelihood, was utilized to generate interspecies phylogenetic trees of RRS1, RARE and UBP12/13 under Poisson substitution model and uniform rates by MEGA 11[63]. On the other hand, the intraspecies phylogenetic tree of WRKY transcription factors was generated using the maximum-likelihood method under the JTT model and gamma distribution by IQ-TREE[64].

For the phylogenetic tree of RRS1 orthologues, the protein sequences used include: *Arabidopsis thaliana*_RRS1-R (C4B7M5), *Arabidopsis lyrata*_RRS1 (XP_020871197), *Capsella rubella*_RRS1 (XP_006279894), *Camelina sativa*_RRS1 like (XP_010494612), *Raphanus sativus*_RRS1 (XP_018455889), *Brassica napus*_RRS1 like (XP_013734065), *Brassica rapa*_RRS1 (LOC103839134), *Brassica oleracea*_RRS1 (XP_013610929), *Arabidopsis thaliana*_CHS3 (NP_197291), *Arabidopsis thaliana*_CSA (NP_197290), *Arabidopsis thaliana*_RPS4 (NP_199338), *Theobroma cacao*_N (XP_017978840), *Eucalyptus grandis*_RPV (XP_010030110), *Vitis vinifera*_N (XP_010661240), *Solanum tuberosum*_NLR (KAH0750703), *Citrus sinensis*_RUN1 like (XP_052293259), *Manihot esculenta*_NLR (KAG8633511), *Citrus clementina*_CICLE (ESR59447), *Carica papaya*_NLR (XP_021909738) and *Gossypium arboreum*_DCS1 (XP_017603119).

For the phylogenetic tree of RARE, the protein sequences used include: *Arabidopsis thaliana*_RARE (NP_001319035), *Capsella rubella*_RARE (XP_006307360), *Brassica rapa*_RARE (XP_009149355), *Citrus sinensis*_RARE (KAH9721972), *Manihot esculenta*_RARE (XP_021592540), *Vitis vinifera*_RARE (WKA08472), *Solanum tuberosum*_RARE (KAH0763893), *Oryza sativa*_RARE (KAF2939895), *Zea mays*_RARE (NP_001169658), *Amborella trichopoda*_RARE (XP_011623580), *Selaginella moellendorffii*_RARE (XP_024528416), *Marchantia polymorpha*_RARE (PTQ47888), *Chlamydomonas reinhardtii*_RARE (XP_042914639), *Dunaliella salina*_RARE (KAF5826418), *Arabidopsis thaliana*_PRT1 (NP_189124) and *Arabidopsis thaliana*_RMA3 (NP_194477).

For the phylogenetic tree of UBP12/13, the protein sequences used include: *Arabidopsis thaliana*_UBP12 (NP_568171), *Capsella rubella*_UBP12 (XP_006289281), *Brassica rapa*_UBP12 (XP_009122271), *Arabidopsis thaliana*_UBP13 (NP_001326292), *Capsella rubella*_UBP13 (XP_006299059), *Brassica rapa*_UBP13 (RID63933), *Citrus sinensis*_UBP12 (XP_006481665), *Manihot esculenta*_UBP12 (XP_021620269), *Vitis vinifera*_UBP12 (XP_002267555), *Solanum tuberosum*_UBP12 (XP_006339190), *Amborella trichopoda*_UBP12 (XP_020522273), *Oryza sativa*_UBP12 (XP_015617197), *Zea mays*_UBP12 (NP_001346364), *Selaginella moellendorffii*_UBP12 (XP_024540510), *Marchantia polymorpha*_UBP12 (PTQ48865), *Chlamydomonas reinhardtii*_UBP12 (XP_042922837), *Dunaliella salina*_UBP12 (KAF5839814), *Arabidopsis thaliana*_UBP26 (NP_001325635) and *Arabidopsis thaliana*_UBP16 (NP_567705).

To generate the phylogenetic tree of WRKY transcription factors, their WRKY domains were identified by the Conserved Domain Database[65] and the protein sequences of WRKY domains were subjected to phylogenetic analysis.

LC-MS/MS analysis

For each biotinylated protein sample, two independent biological replicates were performed and analyzed via LC-MS. LC-MS/MS analysis was performed using an Orbitrap Fusion trihybrid mass spectrometer (Thermo Fisher Scientific) and a nanoflow-UHPLC system (Dionex Ultimate3000, Thermo Fisher Scientific) as previously described[66] with the following modifications. Peptides were trapped to a reverse phase trap column (Acclaim PepMap C18, 5 µm, 100 µm × 2 cm, Thermo Fisher Scientific) connected to an analytical column (Acclaim PepMan 100, C18 3 µm, 75 µm × 50 cm, Thermo Fisher Scientific). Peptides were eluted in a sigmodial gradient of 3–65% acetonitrile in 0.1% formic acid (solvent B) over 90 min at a flow rate of 300 nl/min at 40 °C. The mass spectrometer was operated in positive ion mode with nano-electrospray ion source with an inner diameter of 0.02 mm fused silica emitter (New Objective). Voltage 2200 V was applied via platinum wire held in PEEK T-shaped coupling union with transfer capillary temperature set to 275 °C. The Orbitrap, MS scan resolution of 120,000 at 400 m/z, range 300 to 1800 m/z was used, and automatic gain control was set to 2×10^5 and maximum inject time to 50 ms. In the linear ion trap, product ion spectra were triggered with a data-dependent acquisition method using "top speed" and "most intense ion" settings. The threshold for collision-induced dissociation (CID) and high energy collisional dissociation (HCD) was set using the Universal Method (above 100 counts, rapid scan rate, and maximum inject time to 10 ms). The selected precursor ions were fragmented sequentially in both the ion trap using CID and in the HCD cell. Dynamic exclusion was set to 30 s. Charge state allowed between +2 and +7 charge states to be selected for MS/MS fragmentation.

Peak lists in format of Mascot generic files (.mgf files) were prepared from raw data using MSConvert package (Matrix Science). Peak lists were searched on Mascot server version 2.4.1 (Matrix Science)

against TAIR (version 11) database, a separate in-house constructs database and an in-house contaminants database. Tryptic peptides with up to two possible mis-cleavages and charge states +2, +3, +4 were allowed in the search. The following modifications were included in the search: oxidized Met, phosphorylation on Ser, Thr, Tyr as variable modifications, and carbamidomethylated Cys as a static modification. Data were searched with a monoisotopic precursor and fragment ions mass tolerance 10 ppm and 0.6 Da, respectively. Mascot results were combined in Scaffold version 4 (Proteome Software) and exported to Excel (Microsoft Office).

Statistics and reproducibility

Data from inoculation assays and qPCR assays were expressed as mean ± standard deviation (SD). Statistical analyses were performed using one-way ANOVA followed by Tukey's post hoc test, and graphs were generated by OriginPro software. The corresponding *P*-values can be found in the Source Data. The P value < 0.01 was considered to indicate statistical significance.

In this study, representative experimental results, such as figure(s) 1e, f; 2a–f; 3a–d; 4a, b; 6b–e, were independently repeated three times, producing similar results, with the most representative one being shown.

Reporting summary

Further information on research design is available in the Nature Portfolio Reporting Summary linked to this article.

Data availability

All data supporting the findings of this study are available within the manuscript and its supplementary files. TurboID-based proximity labeling combined with mass spectrometry data generated in this study have been deposited in the ProteomeXchange database under the accession code PXD059418 [https://massive.ucsd.edu/ProteoSAFe/dataset.jsp?task=503dae8aa79d44e2adb291824dc0f01d]. The original data points in graphs and uncropped gel of immunoblotting images are provided in the Source Data files. Source data are provided with this paper.

References

1. Jones, J. D. G., Vance, R. E. & Dangl, J. L. Intracellular innate immune surveillance devices in plants and animals. *Science* **354**, aaf6395 (2016).
2. Jones, J. D. G., Staskawicz, B. J. & Dangl, J. L. The plant immune system: from discovery to deployment. *Cell* **187**, 2095 (2024).
3. Feehan, J. M., Castel, B., Bentham, A. R. & Jones, J. D. Plant NLRs get by with a little help from their friends. *Curr. Opin. Plant Biol.* **56**, 99 (2020).
4. Huang, S. et al. NLR signaling in plants: from resistosomes to second messengers. *Trends Biochem. Sci.* **48**, 776 (2023).
5. Jia, A. et al. TIR-catalyzed ADP-ribosylation reactions produce signaling molecules for plant immunity. *Science* **377**, eabq8180 (2022).
6. Forderer, A. et al. A wheat resistosome defines common principles of immune receptor channels. *Nature* **610**, 532 (2022).
7. Bi, G. et al. The ZAR1 resistosome is a calcium-permeable channel triggering plant immune signaling. *Cell* **184**, 3528 (2021).
8. Sarris, P. F., Cevik, V., Dagdas, G., Jones, J. D. G. & Krasileva, K. V. Comparative analysis of plant immune receptor architectures uncovers host proteins likely targeted by pathogens. *BMC Biol.* **14**, 8 (2016).
9. Kroj, T., Chanclud, E., Michel-Romiti, C., Grand, X. & Morel, J. B. Integration of decoy domains derived from protein targets of pathogen effectors into plant immune receptors is widespread. *N. Phytol.* **210**, 618 (2016).
10. Jubic, L. M., Saile, S., Furzer, O. J., El Kasmi, F. & Dangl, J. L. Help wanted: helper NLRs and plant immune responses. *Curr. Opin. Plant Biol.* **50**, 82 (2019).
11. Contreras, M. P., Ludke, D., Pai, H., Toghani, A. & Kamoun, S. NLR receptors in plant immunity: making sense of the alphabet soup. *EMBO Rep.* **24**, e57495 (2023).
12. Yang, Y. et al. Paired plant immune CHS3-CSA1 receptor alleles form distinct hetero-oligomeric complexes. *Science* **383**, eadk3468 (2024).
13. Gu, B. et al. The integrated LIM-peptidase domain of the CSA1-CHS3/DAR4 paired immune receptor detects changes in DA1 peptidase inhibitors in Arabidopsis. *Cell Host Microbe* **31**, 949 (2023).
14. Williams, S. J. et al. Structural basis for assembly and function of a heterodimeric plant immune receptor. *Science* **344**, 299 (2014).
15. Le Roux, C. et al. A receptor pair with an integrated decoy converts pathogen disabling of transcription factors to immunity. *Cell* **161**, 1074 (2015).
16. Sarris, P. F. et al. A plant immune receptor detects pathogen effectors that target WRKY transcription factors. *Cell* **161**, 1089 (2015).
17. Ma, Y. et al. Distinct modes of derepression of an Arabidopsis immune receptor complex by two different bacterial effectors. *Proc. Natl Acad. Sci. USA* **115**, 10218 (2018).
18. Guo, H. et al. Phosphorylation-regulated activation of the arabidopsis RRS1-R/RPS4 immune receptor complex reveals two distinct effector recognition mechanisms. *Cell Host Microbe* **27**, 769 (2020).
19. Sun, Y., Zhu, Y. X., Balint-Kurti, P. J. & Wang, G. F. Fine-tuning immunity: players and regulators for plant NLRs. *Trends Plant Sci.* **25**, 695–713 (2020).
20. Cheng, Y. T. et al. Stability of plant immune-receptor resistance proteins is controlled by SKP1-CULLIN1-F-box (SCF)-mediated protein degradation. *Proc. Natl Acad. Sci. USA* **108**, 14694–14699 (2011).
21. Liu, J. et al. The malectin-like receptor-like kinase LETUM1 modulates NLR protein SUMM2 activation via MEKK2 scaffolding. *Nat. Plants* **6**, 1106–1115 (2020).
22. Dong, O. X. et al. Individual components of paired typical NLR immune receptors are regulated by distinct E3 ligases. *Nat. Plants* **4**, 699–710 (2018).
23. Wu, Z. et al. Plant E3 ligases SNIPER1 and SNIPER2 broadly regulate the homeostasis of sensor NLR immune receptors. *EMBO J.* **39**, e104915 (2020).
24. Bailey, P. C. et al. Dominant integration locus drives continuous diversification of plant immune receptors with exogenous domain fusions. *Genome Biol.* **19**, 23 (2018).
25. Grund, E., Tremousaygue, D. & Deslandes, L. Plant NLRs with integrated domains: unity makes strength. *Plant Physiol.* **179**, 1227 (2019).
26. Tamborski, J. & Krasileva, K. V. Evolution of plant NLRs: from natural history to precise modifications. *Annu. Rev. Plant Biol.* **71**, 355 (2020).
27. Branon, T. C. et al. Efficient proximity labeling in living cells and organisms with TurboID. *Nat. Biotechnol.* **36**, 880 (2018).
28. Ngou, B. P. M. et al. Estradiol-inducible AvrRps4 expression reveals distinct properties of TIR-NLR-mediated effector-triggered immunity. *J. Exp. Bot.* **71**, 2186 (2020).
29. Saucet, S. B. et al. Two linked pairs of *Arabidopsis* TNL resistance genes independently confer recognition of bacterial effector AvrRps4. *Nat. Commun.* **6**, 6338 (2015).
30. Deslandes, L. et al. Physical interaction between RRS1-R, a protein conferring resistance to bacterial wilt, and PopP2, a type III effector targeted to the plant nucleus. *Proc. Natl Acad. Sci. USA* **100**, 8024 (2003).

31. Mair, A., Xu, S. L., Branon, T. C., Ting, A. Y. & Bergmann, D. C. Proximity labeling of protein complexes and cell-type-specific organellar proteomes in *Arabidopsis* enabled by TurboID. *Elife* **8**, e47864 (2019).
32. Zhu, Z. et al. Arabidopsis resistance protein SNC1 activates immune responses through association with a transcriptional corepressor. *Proc. Natl Acad. Sci. USA* **107**, 13960 (2010).
33. Monaghan, J., Xu, F., Xu, S., Zhang, Y. & Li, X. Two putative RNA-binding proteins function with unequal genetic redundancy in the MOS4-associated complex. *Plant Physiol.* **154**, 1783 (2010).
34. Clague, M. J., Urbe, S. & Komander, D. Breaking the chains: deubiquitylating enzyme specificity begets function. *Nat. Rev. Mol. Cell Biol.* **20**, 338 (2019).
35. Ewan, R. et al. Deubiquitinating enzymes AtUBP12 and AtUBP13 and their tobacco homologue NtUBP12 are negative regulators of plant immunity. *N. Phytol.* **191**, 92–106 (2011).
36. Wang, Y. et al. The IMMUNE-ASSOCIATED NUCLEOTIDE-BINDING 9 protein is a regulator of basal immunity in *Arabidopsis thaliana*. *Mol. Plant Microbe Interact*. https://doi.org/10.1094/mpmi-03-18-0062-r (2019).
37. Kosarev, P., Mayer, K. F. & Hardtke, C. S. Evaluation and classification of RING-finger domains encoded by the Arabidopsis genome. *Genome Biol.* **3**, 0016 (2002).
38. Zhang, H. et al. The RING finger ubiquitin E3 ligase SDIR1 targets SDIR1-INTERACTING PROTEIN1 for degradation to modulate the salt stress response and ABA signaling in *Arabidopsis*. *Plant Cell* **27**, 214 (2015).
39. Castel, B. et al. Evolutionary trade-offs at the *Arabidopsis* WRR4A resistance locus underpin alternate Albugo candida race recognition specificities. *Plant J.* **107**, 1490 (2021).
40. Babu, M. M. The contribution of intrinsically disordered regions to protein function, cellular complexity, and human disease. *Biochem. Soc. Trans.* **44**, 1185 (2016).
41. Trenner, J. et al. Evolution and functions of plant U-Box proteins: from protein quality control to signaling. *Annu. Rev. Plant Biol.* **73**, 93 (2022).
42. Huh, S. U. et al. Protein-protein interactions in the RPS4/RRS1 immune receptor complex. *PLoS Pathog.* **13**, e1006376 (2017).
43. Guo, H., Wang, S. & Jones, J. D. G. Autoactive *Arabidopsis* RPS4 alleles require partner protein RRS1-R. *Plant Physiol.* **185**, 761 (2021).
44. Noutoshi, Y. et al. A single amino acid insertion in the WRKY domain of the *Arabidopsis* TIR-NBS-LRR-WRKY-type disease resistance protein SLH1 (sensitive to low humidity 1) causes activation of defense responses and hypersensitive cell death. *Plant J.* **43**, 873 (2005).
45. Jeong, J. S., Jung, C., Seo, J. S., Kim, J. K. & Chua, N. H. The deubiquitinating enzymes UBP12 and UBP13 positively regulate MYC2 levels in jasmonate responses. *Plant Cell* **29**, 1406 (2017).
46. Lee, C. M. et al. GIGANTEA recruits the UBP12 and UBP13 deubiquitylases to regulate accumulation of the ZTL photoreceptor complex. *Nat. Commun.* **10**, 3750 (2019).
47. Cui, X. et al. Ubiquitin-specific proteases UBP12 and UBP13 act in circadian clock and photoperiodic flowering regulation in *Arabidopsis*. *Plant Physiol.* **162**, 897 (2013).
48. Higashi, K. et al. Modulation of defense signal transduction by flagellin-induced WRKY41 transcription factor in *Arabidopsis thaliana*. *Mol. Genet. Genomics* **279**, 303 (2008).
49. Knoth, C., Ringler, J., Dangl, J. L. & Eulgem, T. *Arabidopsis* WRKY70 is required for full RPP4-mediated disease resistance and basal defense against *Hyaloperonospora parasitica*. *Mol. Plant Microbe Interact.* **20**, 120 (2007).
50. Zhou, Y., Park, S. H. & Chua, N. H. UBP12/UBP13-mediated deubiquitination of salicylic acid receptor NPR3 suppresses plant immunity. *Mol. Plant* **16**, 232 (2023).
51. Zhang, Y. et al. TurboID-based proximity labeling reveals that UBR7 is a regulator of N NLR immune receptor-mediated immunity. *Nat. Commun.* **10**, 3252 (2019).
52. Wang, C. et al. A viral effector blocks the turnover of a plant NLR receptor to trigger a robust immune response. *EMBO J.* **43**, 3650–3676 (2024).
53. Yuan, M. et al. Pattern-recognition receptors are required for NLR-mediated plant immunity. *Nature* **592**, 105 (2021).
54. Ngou, B. P. M., Ahn, H. K., Ding, P. & Jones, J. D. G. Mutual potentiation of plant immunity by cell-surface and intracellular receptors. *Nature* **592**, 110 (2021).
55. Pruitt, R. N. et al. The EDS1-PAD4-ADR1 node mediates *Arabidopsis* pattern-triggered immunity. *Nature* **598**, 495 (2021).
56. Tian, H. et al. Activation of TIR signalling boosts pattern-triggered immunity. *Nature* **598**, 500 (2021).
57. Weir, M. E. et al. Novel autophosphorylation sites of Src family kinases regulate kinase activity and SH2 domain-binding capacity. *FEBS Lett.* **590**, 1042 (2016).
58. Qian, X. et al. The Tensin-3 protein, including its SH2 domain, is phosphorylated by Src and contributes to tumorigenesis and metastasis. *Cancer Cell* **16**, 246 (2009).
59. Xu, F., Xu, S., Wiermer, M., Zhang, Y. & Li, X. The cyclin L homolog MOS12 and the MOS4-associated complex are required for the proper splicing of plant resistance genes. *Plant J.* **70**, 916–928 (2012).
60. Huang, C. Y. et al. The chromatin-remodeling protein BAF60/SWP73A regulates the plant immune receptor NLRs. *Cell Host Microbe* **29**, 425–434 (2021).
61. Liu, G. et al. The deubiquitinases UBP12 and UBP13 integrate with the E3 ubiquitin ligase XBAT35.2 to modulate VPS23A stability in ABA signaling. *Sci. Adv.* **8**, eabl5765 (2022).
62. Guo, H. et al. Plastid-nucleus communication involves calcium-modulated MAPK signalling. *Nat. Commun.* **7**, 12173 (2016).
63. Tamura, K., Stecher, G. & Kumar, S. MEGA11: molecular evolutionary genetics analysis version 11. *Mol. Biol. Evol.* **38**, 3022 (2021).
64. Chernomor, O., von Haeseler, A. & Minh, B. Q. Terrace aware data structure for phylogenomic inference from supermatrices. *Syst. Biol.* **65**, 997 (2016).
65. Wang, J. et al. The conserved domain database in 2023. *Nucleic Acids Res* **51**, D384 (2023).
66. Bender, K. W. et al. Autophosphorylation-based Calcium (Ca^{2+}) sensitivity priming and Ca^{2+}/Calmodulin inhibition of *Arabidopsis thaliana* Ca^{2+}-dependent protein kinase 28 (CPK28). *J. Biol. Chem.* **292**, 3988 (2017).

Acknowledgements

We thank Dr. Xia. Cui from the Chinese Agricultural Academy of Sciences for providing *ubp12-2w* mutant seeds. We also thank Dr. Qian Chen (China Agricultural University) for her help with the in vitro ubiquitination assay. We thank Dr. Robert Heal and Dr. Joe Win from The Sainsbury Laboratory for the suggestions on manuscript improvement and phylogeny analysis, respectively. This research was supported by the National Natural Science Foundation of China (32100239, 32270307 to H.G.), Beijing NOVA Program (Z211100002121066 to H.G.), Marie Skłodowska-Curie scheme (H2020-MSCA-IF-2014-655295 to J.H.) and ERC Advanced Grant "Immunity by Pair Design"(J.D.G.J.).

Author contributions

Conceptualization, H.G., J.H., and J.D.G.J.; Investigation, H.G., Z.C., J.H., J.L., and F.L.H.M.; Writing – Original Draft, H.G. and J.H.; Writing – Review & Editing, H.G., J.H., and J.D.G.J.; Funding Acquisition, H.G., and J.D.G.J.; Supervision, H.G., and J.D.G.J.

Competing interests

The authors declare no competing interests.

Additional information

Supplementary information The online version contains supplementary material available at https://doi.org/10.1038/s41467-025-57231-9.

Correspondence and requests for materials should be addressed to Jonathan D. G. Jones or Hailong Guo.

Peer review information *Nature Communications* thanks Steven Spoel and the other, anonymous, reviewer(s) for their contribution to the peer review of this work. A peer review file is available.